Journal of Thermal Analysis and Calorimetry, Vol. 84 (2006) 2, 503–509

EFFECT OF CERIUM, HOLMIUM AND SAMARIUM IONS ON THE THERMAL AND STRUCTURAL PROPERTIES OF THE HZSM-12 ZEOLITE

Anne M. Garrido Pedrosa[1*], *M. J. B. Souza*[2], *A. O. S. Silva*[3], *Dulce M. A. Melo*[1] *and A. S. Araujo*[1]

[1]Department of Chemistry, Federal University of Rio Grande do Norte, CP1662, 59078-970 Natal, RN, Brazil
[2]Department of Chemical Engineering, Federal University of Sergipe, 49100-000 São Cristovão, SE, Brazil
[3]Laboratory of Catalysis and Environmental, UNIFACS, 40220-141, Salvador, BA, Brazil

The study of the incorporation of rare earth elements as additives in Y zeolites is a very interesting field of research, mainly by its potential application as additives in catalytic cracking process. In this work was studied the thermal and structural properties of cerium, holmium and samarium supported on HZSM-12 zeolite. The obtained materials were characterized by X-ray diffraction (XRD), infrared spectroscopy (FTIR), nitrogen adsorption, thermogravimetry (TG/DTG), differential scanning calorimetry (DSC) and differential thermal analysis (DTA). TG/DSC/DTA analyses showed that the dehydration temperatures of RE/HZSM-12 zeolites (*RE*=Ce, Ho, Sm) increase in relation to pure HZSM-12. The acid properties were investigated by pyridine thermo desorption via TG. The results showed two events of mass loss attributed to elimination of pyridine adsorbed on the weak+medium acid sites and on the strong acid sites.

Keywords: *acid properties, DSC, DTA, HZSM-12 zeolite, rare earth, TG*

Introduction

The ZSM-12 zeolite is a synthetic molecular sieve with one-dimensional 12-membered-rings (12MR) channel system. The three-dimensional four-connected net of vertex-sharing TO_4-tetrahedra (*T*=Si, Al) results in a one-dimensional channel system confined by 12MR with pore openings of about 5.6·5.9 Å. The straight 12MR channel runs parallel to the long crystal axis, i.e. parallel to b_0 of the monoclinic unit cell [1, 2]. This kind of channels is interesting for application in several reactions of industrial interest due to its good stability, resistance to deposition of hard coke and excellent performance in catalytic processes [3–6]. The properties of several molecular sieves containing different rare earths have been studied [7–10] and showed that the presence of rare earth in these systems is responsible for improving thermal stability and catalytic activity in several reactions of interest. The positive effects of the rare earth elements on properties of molecular sieves can be related to the creating a high electric field gradient strong enough to dissociate adsorbed water and provide a surface acidity as also due to the formation of rare earth-oxygen bonds [11]. The thermal properties of molecular sieves containing rare earths have been studied in the literature for several techniques such as TG, DTA and DSC. From these analyses it is possible to study the dehydration, dehydroxylization and collapse temperatures of zeolite samples. Thermal analysis has been also applied to study the acid properties of zeolite catalysts from thermodesorption of bases adsorbed [12–14].

In this paper we have reported the synthesis, characterization and thermal and structural properties of the HZSM-12 containing cerium, samarium and holmium ions. XRD and FTIR techniques were used to investigate structural properties of zeolite samples.

Experimental

The NaZSM-12 zeolite with Si/Al molar ratio of 40 was synthesized under hydrothermal conditions starting from a hydro gel with the following molar composition: $10(MTEA)_2O{:}1.25Al_2O_3{:}10Na_2O{:}100SiO_2{:}200H_2O$.
The MTEA (methyltriethylammonium) was used as structure template. After synthesis the organic template was removed by calcination in N_2 at 823 K for 1 h, and after in air at 823 K for 9 h. Ammonium form of the zeolite was obtained by ion exchange with 1 M NH_4Cl solution at 343 K for 2 h. Finally, the zeolite was converted to their protonated forms by ammonia liberation via calcination in air at 773 K for 4 h. HZSM-12 zeolite containing different rare earth ions were prepared by incipient wetness impregnation. An aqueous solution of cerium, samarium or holmium nitrates was added to 1 g of HZSM-12 zeolite under constant mixing at 343 K. This temperature was maintained constant for 2 h. The rare earth nitrates contents were calculated to a rare earth loading of ca. 5 mass% on the HZSM-12 zeolite. After the impregnation step, the samples were calcined in atmosphere air at 773 K for 1 h.

* Author for correspondence: annemgp@yahoo.com

1388–6150/$20.00

Akadémiai Kiadó, Budapest, Hungary
Springer, Dordrecht, The Netherlands

Energy dispersive analyses were carried out on an EDX-800 instrument. According to chemical analysis, RE/HZSM-12 samples with metal content of 4.7% for Ce/HZSM-12, 5.1% for Sm/HZSM-12 and 4.9% for Ho/HZSM-12 were obtained after the impregnation of these metals on the HZSM-12 support. The X-ray patterns were obtained on a Shimadzu XRD-6000 diffractometer using CuK_α radiation (λ=1.5418 Å). Infrared spectra by Fourier Transformed were recorded using 1–2% of zeolite sample in KBr pellets in an ABB Bomem instrument model MB104. According to FTIR results were observed fundamental vibrations of TO_4 units of the zeolite frameworks and also of the 12MR channel system. Nitrogen adsorption data at 77 K were obtained on Quanta Chrome NOVA 2000 equipment and the total surface areas of the zeolite samples were measured applying BET method [15]. The determination of external and micropore surface areas were determined by *t*-plot method [16]. Thermal analysis (TG and DSC) were carried out on a Shimadzu TGA-50H and on a Shimadzu DSC-50 instruments at a heating rate of 10 K min^{-1} and under nitrogen flowing at a rate of 50 cm^3 min^{-1}. TG measurements were performed using a platinum crucible and about 2.1–2.4 mg of sample; in the DSC measurements was used an aluminum crucible and about 1.5–1.7 mg of sample. DTA curves were recorded in air atmosphere at a rate of 50 cm^3 min^{-1} and at the heating rate of 10 K min^{-1} on a Perkin-Elmer DTA-1700 instrument using α-alumina as reference material and 10.0–11.0–mg of sample. The acid properties of the zeolite samples were investigated by pyridine thermodesorption. The procedure consisted in activated sample at 673 K for 30 min in nitrogen flow. After that the temperature was reduced to 368 K and the sample was saturated with vapors of pyridine for 30 min. The sample saturated with pyridine was purged with nitrogen for 30 min at same adsorption temperature to remove the physically adsorbed base. The pyridine desorption was performed by heating 10 mg of saturated sample in a Mettler TGA-851 instrument at a heating rate of 10 K min^{-1} and under nitrogen flowing at a rate of 25 cm^3 min^{-1}. The catalytic performance of HZSM-12 and RE-HZSM-12 in the *n*-heptane oxidation was evaluated in a fixed bed continuous flow reactor [17]. The process occurred at atmospheric pressure, temperature in the catalytic bed in the range 703–743 K, F/W ratio (molar flux of reactant per mass of catalyst) of 0.51 mol g^{-1} h^{-1} and using a dynamic air atmosphere as carrier gas at a flow of 30 cm^3 min^{-1}. The samples of catalysts used were of 100 mg. The reaction products were analyzed in a CG17A gas chromatograph coupled in a QP5000 mass spectrometer (Shimadzu).

Results and discussion

XRD patterns for the HZSM-12 and RE-HZSM-12 samples are shown in Fig. 1. All the peaks are characteristic of MTW structure closely with the reported ones [18]. MTW structure was characterized by intense peaks with degree and Miller index at 7.55º (101), 8.95º (201) and 20.94º (310). All MTW peaks were attributed to monoclinic unit cells, space group C2/*c* [2, 18, 19]. According to XRD data, no significant changes occurred in the lattice parameters of the MTW structure after impregnation of rare earth ions and the number of diffraction peaks also did not change, indicating that no crystalline transformation occurred during treatment of impregnation of rare earth ions. The presence of rare earth oxide (RE–O) phase along with HZSM-12 crystalline phase could not be observed because RE–O is in small contents on zeolite. The values of total, micropore and external areas for HZSM-12 and RE/HZSM-12 samples are given in Table 1. The impregnation of rare earth ions on HZSM-12 occasioned for all samples a decrease in the total surface area and proportional decreasing in the micropore and external areas. The reduction in the micropore and external areas can be attributed to the partial dealuminization during the process of impregnations and subsequent calcination, which may generate the extra-framework aluminum species inside the pores and channels of the zeolite.

Table 1 Total, micropore and external surface areas of zeolite samples

Sample	Total area/m^2 g^{-1}	External area/m^2 g^{-1}	Micropore area/m^2 g^{-1}
HZSM-12	219	34	185
Ce/HZSM-12	203	35	168
Sm/HZSM-12	191	28	163
Ho/HZSM-12	194	29	165

The FTIR spectra of HZSM-12 and RE/HZSM-12 samples are shown in Fig. 2. These spectra showed fundamental vibrations of TO_4 units of the zeolite frameworks and also of 12MR channel system. The broad band around 1223–1085 cm^{-1} showed in the spectrum of the HZSM-12 is assigned to an asymmetrical stretch of TO_4 tetrahedra (*T*=Si, Al); it is almost unchanged in position in the spectrum of RE/HZSM-12. The absorption bands showed in the region 820–650 and 600–560 cm^{-1} were attributed to symmetric stretching of external tetrahedra and to vibrations of 12MR channel system, respectively. Other bands showed in the spectra between 542–470 cm^{-1} are assigned to T–O bending. The vibration at 1641 cm^{-1} can be assigned to the deformation band of adsorbed water. The spectra of the

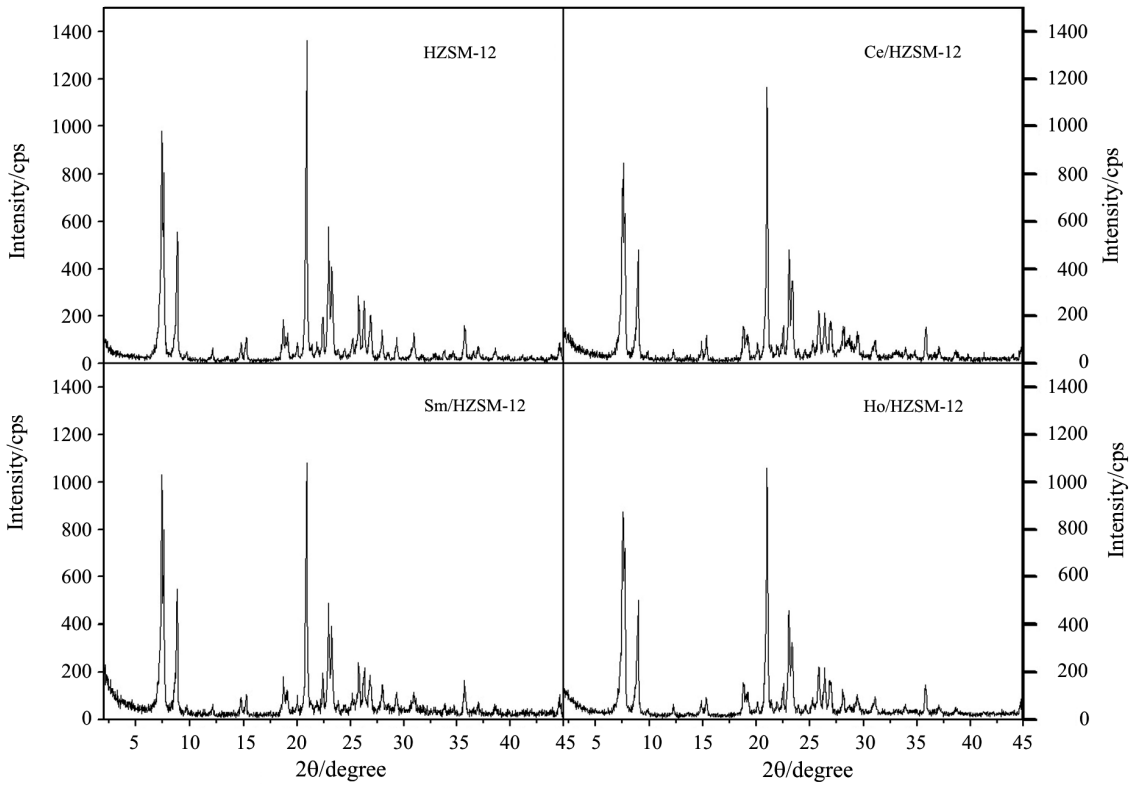

Fig. 1 X-ray powder diffraction pattern of the HZSM-12 and RE/HZSM-12 samples

HZSM-12 and RE/HZSM-12 samples are very similar which indicated that the treatment of impregnation of rare earth ions on the HZSM-12 does not influence the zeolite structure.

Thermal analysis has been found to yield information on the dehydratation and dehydroxylation temperatures of zeolites as also about the thermal stability of the zeolite framework. TG/DTG curves of HZSM-12 and RE/HZSM-12 samples are shown in Fig. 3. TG/DTG curves showed an initial mass loss (about 2–10%) in the temperature range of 303–473 K which is attributed to release water molecules in the large cavities of the zeolite, and the more specific water interacting with the cations. It can be seen from Fig. 3 that the release water molecules starts at same temperature but the complete desorption occurs at different temperatures for RE/HZSM-12 samples, where the temperature required for complete desorption decrease with the decrease of the size of rare earth ions. The dehydration temperature is higher in the RE/HZSM-12 zeolites samples than in the HZSM-12 pure zeolite. This increase in the dehydration temperature of HZSM-12 after incorporation of rare earth is attributed to the formation of rare earth oxide-water bonds. The dehydration event of all zeolites samples is characterized in DSC curves (Fig. 4) by single endothermic peak between 303–454 K. Table 2 summarizes the mass loss, enthalpy change (ΔH) and temperature range for dehydration temperatures. The enthalpy change values are in the range of

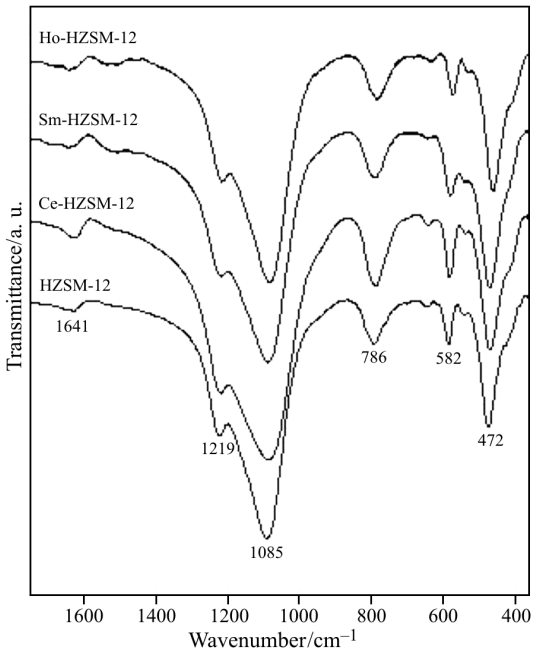

Fig. 2 FTIR spectra of the HZSM-12 and RE/HZSM-12 samples

325.4–482.5 J g^{-1} and also decrease with decrease of the size of rare earth ions. DSC data also suggested that water–cations interactions are lower in the HZSM-12 sample than RE/HZSM-12 samples. Therefore, the incorporation of rare earth ions on the HZSM-12 sample influence on the water molecule interactions and conse-

Table 2 Temperature range (ΔT), mass loss and enthalpy change (ΔH) of the HZSM-12 and RE/HZSM-12 zeolite samples

Sample	TG analysis		DSC analysis	
	ΔT/K	Mass loss/%	ΔT/K	ΔH/J g^{-1}
HZSM-12	303–433	11.7	303–430	325.42
Ce/HZSM-12	303–494	3.8	303–454	482.48
Sm/HZSM-12	303–471	3.6	303–443	339.63
Ho/HZSM-12	303–455	3.4	303–439	335.02

quently in the dehydration temperature range and their ΔH values. In the TG/DTG curves also were observed a second event of mass loss broad and not well-defined showed in the temperature range of 473–1073 K which was attributed to dehydroxylation. The zeolites lost 2–3% of mass in this temperature range due to the dehydroxylation. The dehydration of the zeolite structure was evidenced in the DTA curves (Fig. 5) by single endothermic peak at same temperature range. The exothermic peak showed at about 1307 K in the DTA curves was attributed to a phase transition or collapse of HZSM-12 structure.

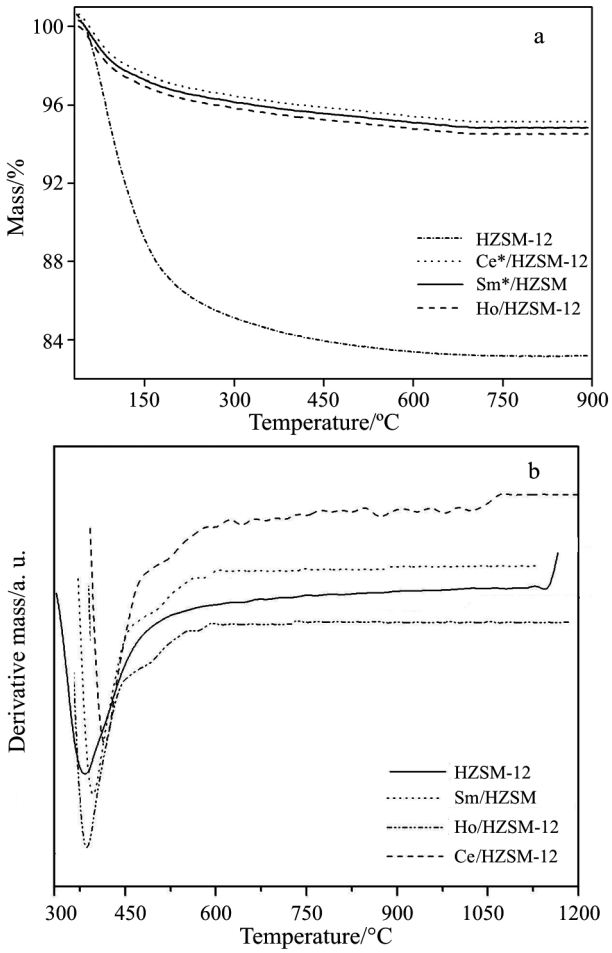

Fig. 3 a – TG and b – DTG curves of the HZSM-12 and RE/HZSM-12 samples

The acid properties of zeolite samples were evaluated by pyridine thermodesorption. Acid sites density per grams of zeolite was correlated with site strength (weak, medium or strong) which is generally attributed in accordance with temperature range of desorption [12, 13]. Figure 6 shows TG/DTG curves of pyridine desorption to HZSM-12 and RE/HZSM-12 samples. It was possible to observe in all cases typically two larger events of mass variation: (*i*) 368–663 K attributed to

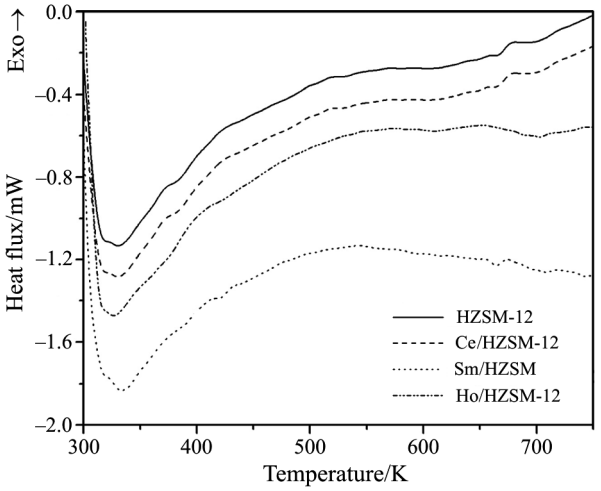

Fig. 4 DSC curves of the HZSM-12 and RE/HZSM-12 samples

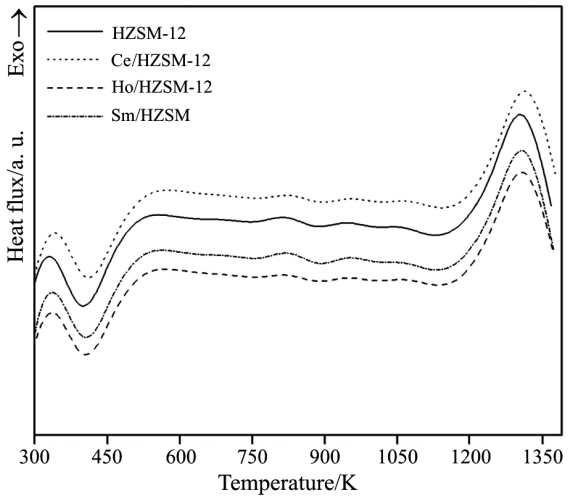

Fig. 5 Differential thermal analysis curves of the HZSM-12 and RE/HZSM-12 samples

elimination of pyridine adsorbed on the weak+medium acid sites and (*ii*) 663–983 K attributed to elimination of pyridine adsorbed on the strong acid sites. The complete desorption of pyridine occurs at different temperatures for RE/HZSM-12 samples indicating that after the incorporation of different rare earth ions in the HZSM-12 zeolite the site strength can be change. The temperature required for complete pyridine desorption decrease with the decrease of the size of rare earth ions. Table 3 shows the temperature range and acid sites density of zeolite samples. In accordance with these results is possible observed that for RE/HZSM-12 samples, the experimental density of strong acid sites is lower than HZSM-12 sample. This decrease in the pyridine adsorption capacity is due to partial blocking effect of the HZSM-12 pore system which is result of presence of rare earth oxides particles inside the HZSM-12 pore system. This partial blocking pore system is mainly attributed to the dealuminization process during the calcinations, which caused a small decrease in the acid site density. Acid values of all zeolites samples are in close agreement with the reported literature to other similar zeolites with high ratio Si/Al [13]. It can be seen from Table 3 that the acid site densities for the RE/HZSM-12 decrease with the decrease of the size.

Catalytic oxidation over several oxides-based catalysts is an important reaction in the petrochemical industry. It offers one of the most efficient means for controlling atmosphere pollution. A graphic of *n*-heptane oxidation as function of temperature is shown in Fig. 7. The *n*-heptane conversion had a gradual increase with increase of reaction temperature for RE/HZSM-12 and HZSM-12 catalysts. Ce/HZSM-12 shows a much higher activity than Sm/HZSM-12 and Ho/HZSM-12. This activity also was much higher when compared with HZSM-12. The low temperatures (703 K) RE/HZSM-12 catalysts showed a catalytic activity higher than

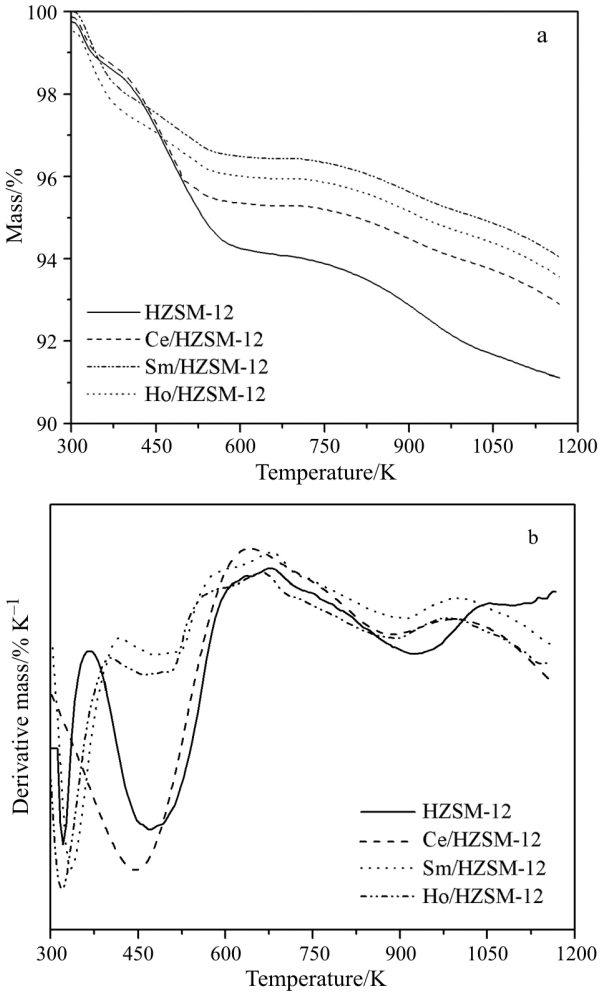

Fig. 6 a – TG and b – DTG curves of pyridine desorption of the HZSM-12 and RE/HZSM-12 samples

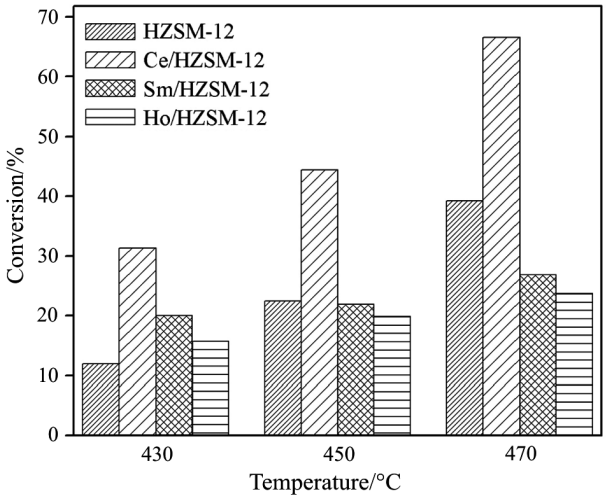

Fig. 7 Total conversion of *n*-heptane *vs*. reaction temperature on HZSM-12 and RE/HZSM-12 samples

Table 3 Temperature range (ΔT) and acid sites density (δ) of the HZSM-12 and RE/HZSM-12 zeolite samples

Samples	Weak+medium sites		Strong sites		δ total/mmol g_{cat}^{-1}
	ΔT/K	δ/mmol g_{cat}^{-1}	ΔT/K	δ/mmol g_{cat}^{-1}	
HZSM-12	311–637	0.56	637–1087	0.39	0.95
Ce/HZSM-12	303–633	0.48	633–1025	0.33	0.81
Sm/HZSM-12	303–621	0.21	621–1013	0.19	0.40
Ho/HZSM-12	303–618	0.12	618–994	0.24	0.36

Table 4 Selectivity products for *n*-heptane oxidation over HZSM-12 and RE/HZSM12 samples

Catalyst	Main products selectivity/%								
	CO_2			CO			C_3*		
	T_1	T_2	T_3	T_1	T_2	T_3	T_1	T_2	T_3
HZSM-12	23.78	17.83	16.44	20.43	14.42	14.54	43.84	58.83	60.74
Ce/HZSM-12	39.90	41.87	43.33	8.21	8.76	8.79	32.93	29.42	25.82
Sm/HZSM-12	34.91	37.64	25.65	10.93	9.81	14.50	37.38	36.62	47.26
Ho/HZSM-12	36.15	38.76	37.89	11.97	12.54	10.97	32.64	30.07	27.06

*C_3=propane+propene; T_1=703 K; T_2=723 K and T_3=743 K

HZSM-12. This situation changes when increase the reaction temperature (from 703 to 723 K). At 723 K, HZSM-12 catalyst has an activity similar to the Sm/HZSM-12 and Ho/HZSM-12. Only at 743 K the catalytic activity of HZSM-12 becomes higher than Sm/HZSM-12 and Ho/HZSM-12. The main products selectivity for *n*-heptane oxidation is given in the Table 4. In accordance with this results not only the conversion but also the selectivity for CO_2 (complete oxidation) is influenced by the reaction temperature. The selectivity to the complete oxidation products decreased with the increasing of the reaction temperature, except for the Ce/HZSM-12 catalyst that showed an inverse behavior. GC-MS analysis showed that the main products of *n*-heptane oxidation were CO_2, CO and C_3 (propane and propene) hydrocarbons and also was observed a very small amount of other hydrocarbons in the range of C_2 (ethane and ethene) and C_4 (butanes and butanes).

A typical monomolecular cracking mechanism involves the direct protonation of the *n*-heptane by the acid sites of the HZSM-12 zeolite to form a high-energy transition state, which subsequently cracks or dehydrogenates to yield an alkane and an alkene [20]. These hydrocarbons and its intermediates under oxidant atmosphere produce CO and CO_2 by incomplete and complete combustion, respectively. As showed in Table 4 the presence of rare earth oxides as addictives on the HZSM-12 zeolite causes an increase in the CO_2/CO ratio in comparison with the pure HZSM-12. The high activity and selectivity of Ce/HZSM-12 in relation to Sm/HZSM-12 and Ho/HZSM-12 in the *n*-heptane oxidation suggested an important role of Ce^{4+} ions in the catalytic process. This can be explained on the basis in the fourth ionization potentials of rare earth, which may be taken as a measure of stability of tetravalent ions relative to the trivalent ions. There is a strong correlation between the fourth ionization potentials and catalytic activity. This correlation has been rationalized by assuming that the rate-determining step of catalytic reaction is the oxidation of the trivalent ion to the tetravalent ion. Similar results were reported by Hattori [21] for rare earth oxides.

Conclusions

The rare earth ions as addictives on the HZSM-12 zeolite influenced on the thermal, structural and catalytic properties of HZSM-12 zeolite. X-ray diffractograms and FTIR spectra showed that in the RE/HZSM-12 samples the structure is still MTW type. The presence of rare earth ions on the HZSM-12 zeolite influence in the dehydration temperatures range and their enthalpy change values. TG/DSC data showed that the temperature and enthalpy change required for complete desorption of water decrease with the decrease of the size of rare earth ions. DTA analyses indicated that at 1307 K a phase transition occurred and could be attributed to the collapse of HZSM-12 structure. The incorporation of rare earth ions on the HZSM-12 sample causes a decreased in the experimental density of acid sites. This can be explained on the basis of partial blocking effect of the HZSM-12 pore system due to dealuminization process. Theses zeolites samples showed a good performance in the *n*-heptane oxidation. Ce/HZSM-12 shows a much higher activity and selectivity than other RE/ZSM-12 zeolite. This high activity and selectivity is attributed to the stability of cerium tetravalent ions.

Acknowledgements

The authors acknowledge to the Conselho Nacional de Desenvolvimento Científico e Tecnologico (CNPq) for its financial support.

References

1 R. B. LaPierre, A. C. Rohrmann, J. L. Schlenker, J. D. Wood, M. K. Rubin and W. J. Rohrbaugh, Zeolites, 5 (1985) 346.
2 C. A. Fyfe, H. Gies, G. T. Kokotailo, B. Marler and D. E. Cox, J. Phys. Chem., 94 (1990) 3718.
3 W. Zhang and P. G. Smirniotis, J. Catal., 182 (1999) 400.
4 S. Gopal and G. Smirniotis, J. Catal., 205 (2002) 231.
5 K. Yoo, E. C. Burckle and G. Smirniotis, J. Catal., 211 (2002) 6.
6 S. Gopal and G. Smirniotis, Appl. Catal. A, 8544 (2003) 1.

7 A. S. Araujo and M. Jaroniec, J. Colloid Interface Sci., 218 (1999) 462.
8 A. S. Araujo, J. M. F. B. Aquino, M. J. B. Souza and A. O. S. Silva, J. Solid State Chem., 2003 (171) 371.
9 F. E. Trigueiro, D. F. J. Monteiro, F. M. Z. Zotin and E. Falabella Sousa-Aguiar, J. Alloys Compd., 344 (2002) 337.
10 F. Lemos, J. M. Lopes and F. Ramoa Ribeiro, Appl. Catal., 49 (1989) 175.
11 Molycorp, Inc.,Cerium: a guide to its role in chemical technology, USA 1995.
12 S. J. Kulkarni and C. V. Kavedia, Thermochim. Acta, 246 (1994) 71.
13 A. M. Garrido Pedrosa, M. J. B. Souza, D. M. A. Melo, A. G. Souza and A. S. Araujo, J. Therm. Anal. Cal., 79 (2005) 439.
14 R. R. C. Pinto, M. L. M. Valle and E. F. Sousa-Aguiar, J. Therm. Anal. Cal., 67 (2002) 439.
15 S. Brunauer, P. H. Emmett and E. Teller, J. Am. Chem. Soc., 60 (1938) 309.
16 J. H. DeBoer and B. C. Lippens, J. Catal., 4 (1965) 319.
17 A. S. Araujo, T. B. Domingos, M. J. B. Souza and A. O. S. Silva, React. Kinet. Catal. Lett., 73 (2001) 283.
18 W. M. Meier, D. H. Olson and C. Baerlocher, Atlas of zeolite structure types. Elsevier; New York 1996.
19 JCPDS, International Center for Diffraction Files, 2000.
20 Y. G. Adewuyi, D. J. Klocke and J. S. Buchanan, Appl. Catal., 131 (1995) 121.
21 T. Hattori, J. Inoko and Y. Murakami, J. Catal., 42 (1976) 60.

Received: March 20, 2005
Accepted: July 20, 2005
OnlineFirst: December 12, 2005

DOI: 10.1007/s10973-005-6911-5